

# Meshing for velocity modeling and ray tracing in complex velocity fields

Andreas Rüger\* and Dave Hale, Landmark Graphics

## Summary

We automatically generate meshes of subsurface velocity structures from finely sampled uniform velocity grids without providing external additional constraints such as horizons and faults. Unlike uniform grids, these new meshes provide a topological framework that enables rapid editing of velocity models, while facilitating numerical tasks such as seismic modeling and inversion.

To minimize traveltimes errors, mesh element size varies according to local velocity complexity. If velocity gradients exceed a specified threshold, we align mesh elements alongside gradient-highs, such as those occurring at sediment-salt interfaces. We may then extract interfaces used for mesh alignment as triangulated surfaces and use them to represent discontinuities in property modeling and seismic ray tracing, or for testing consistency between velocity discontinuities and a depth migrated image.

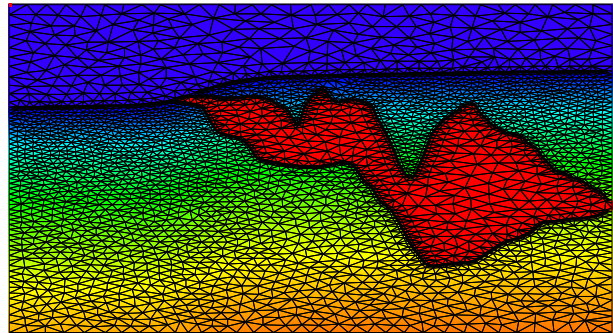
We generate these new velocity meshes in a few minutes of computer time for three-dimensional models. Using finely sampled velocity grids as references, we show that meshes can represent both smooth and discontinuous velocity profiles accurately and with less computer memory than grids.

## Introduction

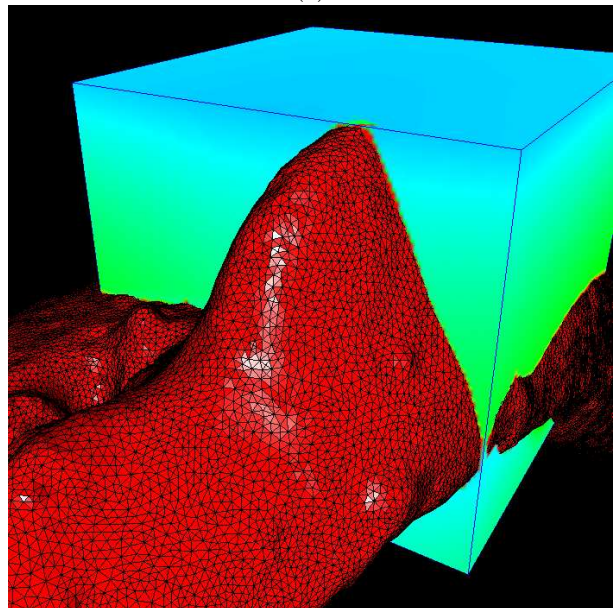
In seismic processing, velocity fields are commonly represented as finely sampled Cartesian grids. This regular discretization of velocity models simplifies some computations, but has drawbacks, such as:

- Oversampling in areas where velocity varies only slightly and where the seismic method cannot resolve rapid variations in velocity.
- No explicit surfaces. Although visible to the human eye, velocity discontinuities in a uniform grid are implicit. Without explicit surfaces, it is difficult in ray tracing, for example, to decide whether to reflect or transmit a ray.
- Awkward editing. Manipulating uniform 3D grids interactively is cumbersome.

Several authors investigate various tessellation-based velocity model representations for tomographic inversion (e.g., Cox and Verschuur, 2001; Böhm, 2000) and methods to create topologically consistent, editable models for applications such as seismic raytracing (Wiggins et al, 1993; Stankovic and Albertin, 1995). Here, we address meshing research from a different angle. First, we demonstrate



(a)



(b)

FIG. 1: (a) Meshing of the  $1200 \times 1000$ -sample Sigsbee velocity model. The superimposed mesh of triangles has about 3000 nodes. (b) Triangulated salt-sediment interface extracted from the mesh of the 3D SEG/EAGE salt model, shown together with a subset of the uniform grid.

that we can accurately describe a highly-resolved velocity field by piecewise-linear interpolation within properly sized and placed mesh elements. Second, we propose a process that can turn a specified finely and uniformly sampled velocity grid into an equivalent mesh.

Results from this process are illustrated in Figure 1a, which shows a 2D triangular mesh overlaying the finely sampled velocity grid of the Sigsbee escarpment in the deep water Gulf of Mexico. The density of the mesh el-

## Meshing for complex velocity fields

ements automatically adjusts to the magnitude of local change in velocity and is highest at the water-sediment and sediment-salt interfaces. These interfaces are embedded in the mesh and can be extracted as shown in Figure 1b for the salt-sediment interface in the SEG/EAGE 3D salt model.

Most mesh-based velocity model building tools are supplemented by nodes on previously interpreted boundary surfaces that need to be combined in a topologically-consistent manner. This can be a tedious process and, while the surfaces are accurately represented, often yields rather coarse velocity approximations between interfaces. In contrast, the *atomic meshing* (Hale, 2002; Hale and Emanuel, 2002) approach discussed below does not depend on externally-provided horizons (although this information can be incorporated), and allows one to insert great detail anywhere in mesh. This new approach also addresses well-known difficulties of edge-preserving meshing (Fomel, 1997), by not representing discontinuity surfaces as edges in a triangulation (2D) or faces in a tetrahedralisation (3D), but still embedding these surfaces topologically in the mesh.

### Atomic meshing

We adapt the atomic meshing process previously used for flow simulation and image segmentation by Hale and Emanuel (2002) to meshing of velocity fields in two or three dimensions (for clarity, examples shown in the paper are 2D). We compute the locations of mesh nodes (*atoms*) by minimizing the sum of two potential energies: (1) one describing inner-atomic attractive and repulsive forces (to guarantee that nodes are not clustered too closely or spread too far apart) and (2) another computed from the velocity field, which aligns atoms alongside discontinuities in velocity.

We begin by applying a standard edge-detection algorithm to highlight velocity discontinuities, as shown in Figure 2b, which was computed for a 2D velocity distribution from the Southern Gas Basin of the North Sea (Figure 2a). Then, we compute a potential field with minima alongside and parallel to those discontinuities. As we minimize our potential energy sum, these potential valleys will attract nearby atoms, thereby forcing atoms to align alongside velocity discontinuities. Before minimizing the total potential energy, we must determine the density of atoms required to adequately describe the change of velocity in each part of the model. Near interfaces, we want more atoms. Also, we should choose the spacing  $d$  between atoms to minimize the traveltime error that could occur if we were to use a constant velocity over that distance:

$$t_{err} = \frac{1}{4} k d^2, \quad (1)$$

where  $k$  denotes the gradient in slowness. For a specified  $t_{err}$ , we use equation (1) to compute the spacing  $d$  between atoms for each sample of the velocity field. As shown in Figure 2c, this computation yields a coarse spacing of atoms (blue) in areas with little change in velocity,

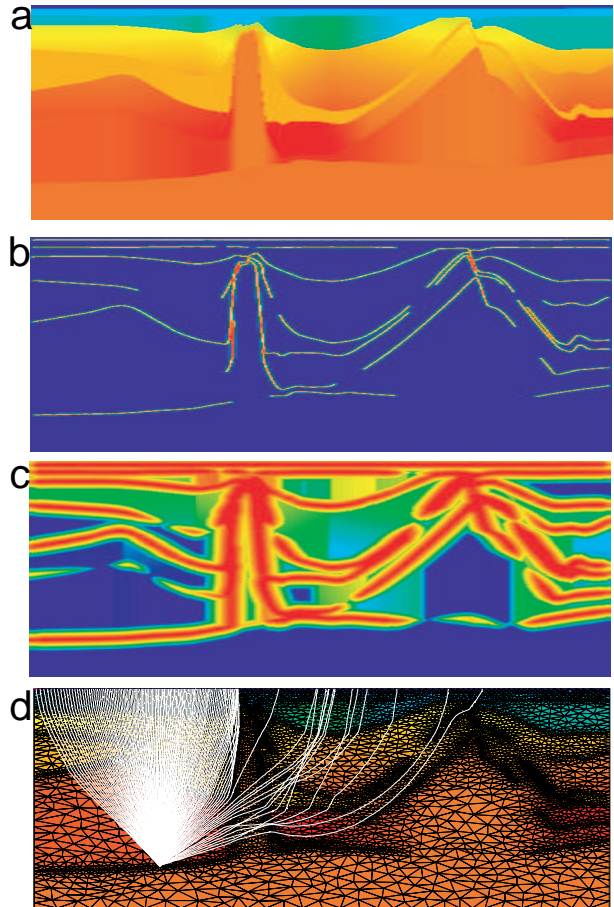


FIG. 2: Processing sequence for a velocity field from the Southern Gas Basin of the North Sea. (a) The uniform ( $1000 \times 1094$ -sample) grid with velocities ranging from  $1500m/s$  to  $6130m/s$ . (b) Output of the edge-detection process. (c) Density of atoms computed from velocity gradients and discontinuities. (d) Final mesh of triangles, shown with the original velocity field and seismic rays traced from a point source. The mesh of triangles has 4684 nodes.

clustering of atoms (red) close to discontinuity surfaces, and intermediate spacing in layers with slightly changing velocities (yellow and green). A distribution like that in Figure 2c guides an initial pseudo-random placement of atoms. Then, as the total potential energy is minimized, atoms align alongside velocity discontinuities. Finally, a Delaunay triangulation of atom locations yields a mesh like that shown in Figure 2d (here used for seismic ray-tracing from a point source in the subsurface).

### Property modeling

Values specified at three nodes of a triangle (or four nodes of a tetrahedron) define a property field that varies linearly within each mesh element and changes continuously

## Meshing for complex velocity fields

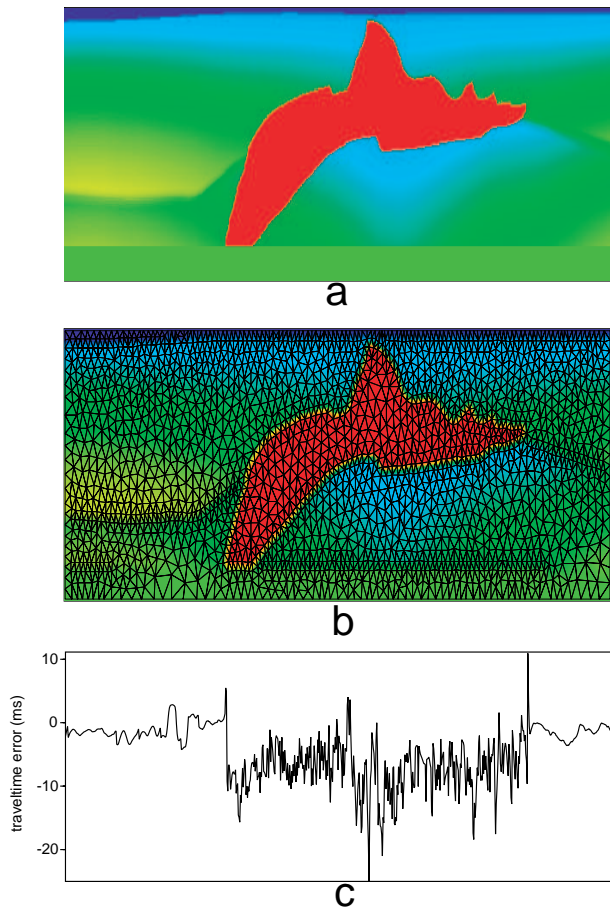


FIG. 3: (a) Slowness field of line AA of the SEG/EAGE Salt model, represented by  $209 \times 780$ -samples. (b) Approximate slowness field obtained by triangulation of 2010 nodes and smooth interpolation within each triangle. The minimum triangle edge length is seven samples; the average length is 10 samples. (c) Traveltime error (exact minus approximate) as a function of horizontal position for rays traveling vertically from the top to the bottom of the model.

between them. At each of our mesh nodes, we specify the value of inverse-velocity-squared (sloth), because linear sloth corresponds to simple and efficient parabolic ray paths within each mesh element (e.g., Chapman and Keers, 2002). To obtain the values of sloth at each mesh node, we simply extract the velocity value from the nearest sample in the uniform grid.

We studied the accuracy of piecewise linear interpolation of sloth by comparing the slowness field of line AA of the SEG/EAGE Salt model (Figure 3a) with a mesh of triangles, where the minimum triangle edge length (distance  $d$  above) is seven samples (Figure 3b). The uniform grid has  $780 \times 209$  samples. The mesh with 2010 nodes closely approximates the original input field and smoothly interpolates the velocity contrast at the salt boundary. We

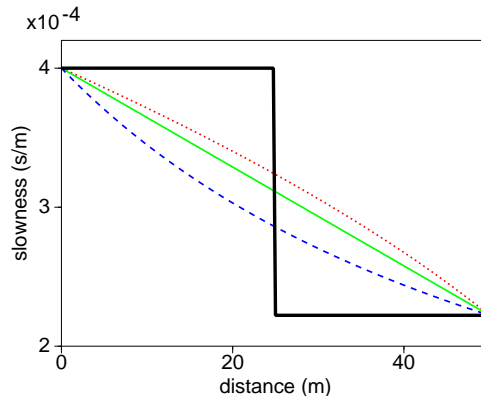


FIG. 4: Slowness profiles along a triangle edge. The exact slowness curve with a discontinuity at the center of the edge is given in black. Also shown are slowness curves corresponding to interpolation with linear slowness (green, solid), linear sloth (red, dotted) and linear velocity (blue, dashed). Integrating over any of these curves yields the traveltime for the corresponding interpolation method. The traveltime is exact for linear slowness, overestimated for linear sloth and underestimated (with larger error) for linear velocity.

then quantified errors by computing traveltimes (integrals of slowness) for rays traveling vertically from the surface to the bottom of the model. Here, we vertically integrated over all samples at each horizontal position in both the exact and approximate slowness fields, and display the differences in Figure 3c. Precise sampling of the slowness values at the salt-sediment interface is impossible, because an infinitesimal change in position yields either the sediment or salt value. Therefore, we see a high frequency component in the errors, with spikes at surface locations coinciding with a near vertical salt-sediment contact. The median absolute error observed is 3.39ms. We also note a bias towards negative errors. We observed this pattern, albeit with less magnitude, in several models where rays travel through salt. This bias is the result of aligning nodes of our mesh alongside (as opposed to precisely on top of) slowness discontinuities, thereby causing triangles to straddle those discontinuities. To understand this bias in traveltime errors, consider a jump in slowness at the midpoint of a triangle edge. This jump is depicted as a thick black line in Figure 4, which also illustrates possible approximations at discontinuities such as the salt boundary. Integrating over either of the curves shown yields the traveltime for each interpolation method. The traveltime is exact for linear slowness (green, solid), overestimated for linear sloth (red, dotted) and underestimated (with larger magnitude) for linear velocity (blue, dashed).

### Discontinuities

Forcing a mesh to include certain boundary edges is a nontrivial problem, with less than ideal solutions (in particular in 3D). Some solutions relax the Delaunay criterion or add additional nodes (e.g., Fomel, 1997). Most

## Meshing for complex velocity fields

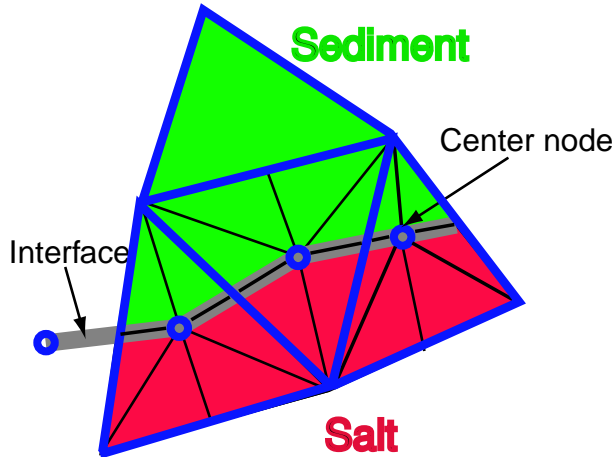


FIG. 5: Splitting of triangles at slowness discontinuities. Triangles with blue edges are part of the Delaunay tessellation; the embedded triangles with black edges are auxiliary triangles and only exist at discontinuities.

solutions represent the discontinuity by edges in the tessellation. This coupling can yield an overly refined mesh and an unstable meshing process. For example, it may be difficult to apply smoothing and similar processes to surfaces without destroying many triangles and causing a re-triangulation. Another problem is that boundary nodes need to hold more than one velocity value. We avoid these problems by not forcing the edges of triangles to coincide with velocity discontinuities. Instead, we internally split triangles that straddle those discontinuities into six sub-triangles, each with a common node in the triangle center and having either, say, salt or sediment properties. (See Figure 5.) The center nodes define a polygon that smoothly approximates the boundary implied by the discontinuity in velocities.

This embedding of a surface in our mesh creates new edges (the thick gray lines in Figure 5) that we may use to reflect or transmit seismic rays. It also removes any bias in traveltime error, as shown in Figure 6b, which we computed for the discontinuous approximation to velocity shown in Figure 6a. The mean absolute error is 2.15ms, a typical value for the series of tests that we performed. We consider this to be an acceptable error for most seismic applications.

### Conclusion

Space-filling, editable meshes are an attractive alternative to finely and uniformly sampled velocity fields. Unlike uniformly sampled grids, unstructured meshes specify detail only where required, thereby reducing memory and computation time for various computational tasks such as ray tracing. The advantages of a mesh-based, editable velocity field, coupled with simple and efficient ray tracing within mesh elements, should lead to improvements in seismic velocity modeling, traveltime estimation and

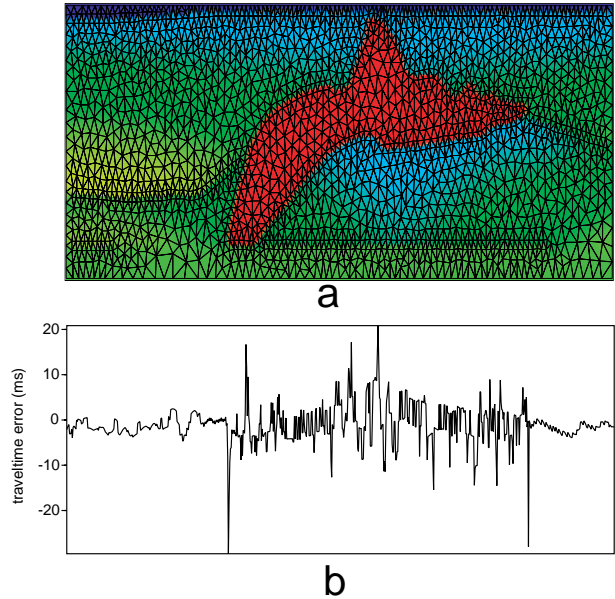


FIG. 6: (a) Approximate slowness field obtained by triangulation of 2010 nodes and splitting of triangles that straddle velocity discontinuities. (b) Vertical traveltime error (exact minus approximate) as a function of horizontal position.

tomography.

### References

- Böhm, G., 2000, 3D adaptive tomography using Delaunay triangles and Voronoi polygons: *Geophysical Prospecting*, 2000, 48, 723-744.
- Chapman, C. H., and Keers, H., 2002, Application of the Maslov seismogram method in three dimensions: *Stud. Geophys. Geod.*, 46, 615-649.
- Cox, B. E., and Vershuur D. J., 2001, Tomographic inversion of focusing operators: In *Expanded Abstracts, M035*, Eur. Assoc. Expl. Geophys.
- Fomel, S., 1997, A variational formulation of the fast marching eikonal solver: *Stanford Exploration Project report 95*, 127-148.
- Hale, D., 2002, Atomic meshes - from seismic imaging to reservoir simulation: *Proceedings of the 8th European Conference on the Mathematics of Oil Recovery*.
- Hale, D., and Emanuel, J., 2002, Atomic meshes of seismic images: presented at the 72nd Ann. Internat. Mtg., Soc. Explor. Geophys.
- Stankovic, G. M., and Albertin, U. K., 1995, Raytracing in topological tetrahedral models: 65th Annual Internat. Mtg., Soc. Expl. Geophys., *Expanded Abstracts*, 1247-1250.
- Wiggins, W., Albertin, U. K., and Stankovic, C., 1993, Building 3-D depth migration velocity models with topological objects: 63rd Annual Internat. Mtg., Soc. Expl. Geophys., *Expanded Abstracts*, 170-173.